ISSN 1330–0008
CODEN FIZAE4

SLIDING SPIN-DENSITY WAVES: STUDIES OF CONDUCTION NOISE, MAGNETIC FIELD DEPENDENCE AND HALL RESISTIVITY

M. BASLETIĆ[a], N. BIŠKUP[b,c], B. KORIN-HAMZIĆ[b], A. HAMZIĆ[a] and S. TOMIĆ[b]

[a] *Department of Physics, Faculty of Science, Bijenička 32, HR-10000 Zagreb, Croatia*

[b] *Institute of Physics, Bijenička 32, HR-10000 Zagreb, Croatia*

[c] *Florida State University, Tallahassee, Florida, USA*

Dedicated to Professor Boran Leontić on the occasion of his 70$^{\mathbf{th}}$ birthday

Received 22 November 1999; revised manuscript received 1 February 2000
Accepted 28 February 2000

We have studied the current-voltage characteristics of the $(TMTSF)_2PF_6$ in the spin density state (SDW), and in zero and finite external magnetic field. For the oscillating part of the nonlinear voltage response to the applied DC electric field, the fundamental frequency distribution (as a function of this field) and a nonlinear relation between the frequency and the SDW current reveal the growth of parallel conduction channels characterized by lower velocities and larger cross-sections. The number of fundamental frequencies, their amplitude and the level of low-frequency noise as well as the depinning behaviour provide a consistent indication of the sample inhomogeneities and associated local field variations, and might be well understood within the framework of the phase slippage model. The increase of the threshold electric field with the applied magnetic filed can be explained by the Bjeliš-Maki theory, if the imperfect nesting is taken into account. Finally, the electric-field dependence of the Hall resistivity is consistent with the sliding mechanism of the SDW conduction.

PACS numbers: 74.70.Kn, 72.15.Nj, 75.30.Fv, 72.70.+m, 72.15.Gd UDC 538.945
Keywords: organic superconductors, collective modes, one-dimensional conductors, spin-density waves, noise processes, galvanomagnetic and other magnetotransport effects

1. *Introduction*

The dynamics of the incommensurate spin-density waves (SDW), found in the systems of reduced dimensionality, has been in the focus of interest in the last ten years. Up to now, the main features which characterize collective response of

the charge-density waves (CDW) have been also experimentally established for the SDW [1,2]. Both types of periodically modulated densities (DW) are pinned to the background lattice by the randomly distributed defects. The oversimplified model considers DW as a one-degree-of-freedom object which moves in a periodic potential $V(2k_{\mathrm{F}}x + \phi)$, where ϕ is the phase of the condensate and k_{F} is the Fermi vector in the chain direction. It is important to observe that in the case of $2k_{\mathrm{F}}$ SDW, the associated modulated charge density has a $4k_{\mathrm{F}}$ periodicity. The effect of an applied electric field, larger than the depinning threshold value, is to tilt the periodic potential and allow the DW to roll down. Such a motion gives rise to a periodic, but non-sinusoidal time-dependent DW current, and its frequency characteristics, as well as its dependence on some external parameters are elaborated in this paper. The time dependence of the DW current defines, in the Fourier space, a fundamental 'washboard' frequency and higher harmonics. In the Fukuyama-Lee-Rice approach [3], the randomly-positioned defects in the real system are taken into account, which implies the treatment of the DW as a deformable object with a broad distribution of phase modes in the defect potential $V(2k_{\mathrm{F}}x + \phi(x))$. It has also been suggested that the coupling of the random phase oscillations leads to their final suppression [4]. However, the numerical calculations have succeeded to recover oscillations only by applying an external AC field [5]. In other words, the theories, which invoke the interaction of the sliding DW with the impurities as the source of the oscillations, have difficulties to explain this phenomenon in the real systems. In an alternative approach, the moving SDW condensate is suppressed at the strong defects and converted into the normal current. At the surface, which separates the sliding and non-sliding regions, a localized annihilation of the order parameter occurs, with a concomitant phase slip by 2π. Several independent theories have been advanced to explain the DW to ohmic current conversion through the formation of DW deformations like phase vortices and dislocation lines [6–11], where their periodic creation and annihilation generates the oscillations of the current.

The conduction noise is one of the most remarkable phenomena associated with the DW motion. In CDW, two different types of oscillations have been observed: *(i)* a well-defined narrow-band noise and *(ii)* a broad-band noise (with $1/f$ dependence). A tight correlation between these oscillations has been pointed out [12–14], but a definite understanding of their origin and their mechanism is still missing. On the other hand, not much is known about the conduction noise that should accompany the SDW sliding. The observed voltage oscillations were either extremely small in amplitude, or very broad in frequency when compared to those in the CDW [15–19]. The only quantitative determination (done in a rather restricted frequency range and on a quite broad Fourier structure) claimed that the narrow-band frequency distribution scaled linearly with SDW current. The different results [18,19] for the ratio between the frequency of the voltage oscillations and the SDW phase rate leave open the question of the origin of the conduction noise in the sliding SDW state. As for the broad-band noise, no clear evidence for its existence in SDW has been reported until now.

The other interesting issue is the effect of the transverse magnetic field on the parameters that characterize the SDW transport. The standard mean-field theory

for a quasi–one-dimensional system with an open Fermi surface (FS) describes well the SDW state [20], that is stabilized by a perfect nesting of the FS. Deviations from the perfect nesting lead to a gradual destruction of the SDW phase. The degree of nesting can be experimentally controlled by the application of hydrostatic pressure and/or magnetic field. The former increases the deviation from perfect nesting while the latter makes it better. The investigations [21] of the phase-coherence length in the SDW state of $(TMTSF)_2NO_3$, a Bechgaard salt with the strong imperfect nesting, have shown that the threshold field increases if a magnetic field is applied in the plane perpendicular to the highly conducting axis (more precisely, only the field component parallel to the lowest conductivity (**c***) axis gives rise to this effect). These results were interpreted in terms of the Bjeliš-Maki theoretical model [24], where the reduction of the longitudinal phase-coherence length in a magnetic field is common to the SDW state with large imperfect nesting.

In this paper we report studies of the sliding spin-density wave phase of the organic conductor $(TMTSF)_2PF_6$. We have studied the current–voltage characteristics and the features of the noise spectra and their dependence on the applied electric field, thermal history of the sample and sample purity. We have also compared the noise spectra detected at different sample segments. These data are analyzed within the framework of the two opposed theoretical models invoking DW-impurity interactions and DW-normal current conversion (phase-slips) as a possible origin of the conduction noise associated with the sliding of density waves. On the other hand, the recently observed [25] variation of the SDW transition temperature and the order parameter of $(TMTSF)_2PF_6$ as a function of pressure and magnetic field, has revealed that the FS nesting at ambient pressure deviates slightly from a perfect one, contrary to the previously accepted opinion. We have, therefore, examined the degree of the perfect nesting deviation in this compound by studying the magnetic field dependence of its threshold field at ambient pressure. We have also extended this work to the linear and non-linear Hall effect to see the effects of the sliding SDW on the Hall voltage.

2. Experiment

The measurements have been performed on single crystals of $(TMTSF)_2PF_6$, grown by a standard electrochemical method. A typical sample resistance at 4.2 K was about 7 Ω. The contact resistances at 4.2 K varied between 10% and 50% of the sample resistance value, depending on the sample and thermal cycling treatment. Annealed gold wires of 20 μm were glued with the silver paint on previously evaporation-deposited gold contacts. We employed a very slow cooling rate (2 – 4 K/h), in order to avoid microcracking of the sample (and the corresponding jumps in the resistance) during the cooldowns. The SDW transition temperature was $T_c = 12.5$ K. Resistance ratios (rr) of the room temperature (RT) resistance to the resistance minimum just above T_c were about 40, and varied within 10% between two consecutive thermal cyclings. Checks for intrinsic nonlinearity did not show any nonlinear effects in the normal high-temperature phase.

For the conduction noise experiment, eight samples have been studied and in five

of them the conduction noise has been found. In some of them, in which the noise pattern was observed, the increase of resistance caused by microcracks was about 10% of the sample resistance at 100 K. The sample selected for the detailed study was 1.5 cm long (in further text denoted as a distance between outer contacts) and had a cross-sectional area of 10^{-4} cm^2. The distance between the voltage contacts (in further text denoted as inner contacts) was 0.34 cm. The measurements of the collective conductivity and the conduction noise were done at $T = 4.2$ K, after different thermal cycling of the samples. The first set of data (run I) was obtained after cooling of the virgin sample from the room temperature down to 4.2 K. The second run (II) was carried out after completing the thermal cycling from 4.2 K up to the room temperature and then down again to 4.2 K. The current–voltage characteristics were measured with the four- and two-terminal arrangements, where the latter was used to detect the conduction noise signal in different independent sections of the sample.

The resistivity was measured with the standard low-frequency AC and DC techniques. The electric-field-dependent conductivity and the Hall effect (in magnetic fields up to 9 T) were measured by the same DC method. To investigate the conduction noise, a battery and a variable resistance were used in series with the sample as the DC current source. The time-dependent portion of the voltage response across the sample was removed and amplified 100 times by a wide-band preamplifier *EGG 115*. A spectral analysis of the voltage output was made using a spectrum analyzer *HP 3588A* with the DC current held at a number of constant values.

3. Results

3.1. Conduction noise

In this section we report the results of experiments on the electric-field dependent conductivity and the associated noise in the sliding SDW phase of $(TMTSF)_2PF_6$. Figure 1 shows the electric-field-dependent conductivity normalized to the low-field ohmic conductivity (σ_0), measured in run I and run II. A strong nonlinearity observed above the threshold field is in agreement with the previously published result [25]. In run I the threshold field is extremely sharp and equals $E_T = 1.8$ mV/cm (which corresponds to the current $I_T = 80$ μA). Note also that the SDW conductivity increases linearly with field up to at least $5E_T$. After a thermal cycling loop (from 4.2 K up to RT and again down to 4.2 K), the low-field sample resistance at 4.2 K was 70% larger than in run I, while the rr was only 10% smaller. The field dependence of the conductivity is smoother and its magnitude for a particular field is smaller. Note that the linear extrapolation of the high-field behaviour does not coincide with the beginning of the conductivity rise. These two points define the depinning threshold region between 3 mV/cm and 6.5 mV/cm (with the corresponding low and high threshold currents being $I_{1T} = 85$ μA and $I_{2T} = 185$ μA, respectively). This is in contrast to the behaviour in run I that gave one, well defined E_T. The two-probe measurements (in which the SDW flow was limited between the inner contacts or the outer contacts) yielded essentially the same result as far as the sharpness of the depinning behaviour is concerned.

The important quantitative difference in run II is a much lower value of the critical current I_{1T} in the two-probe experiment in comparison with the critical current I_{1T} observed in the four-probe experiment, i.e., the enlargement of the depinning region. Such a result indicates that the part of the sample that belongs to the contact area experiences a much higher field than its average value through the sample (the bulk value).

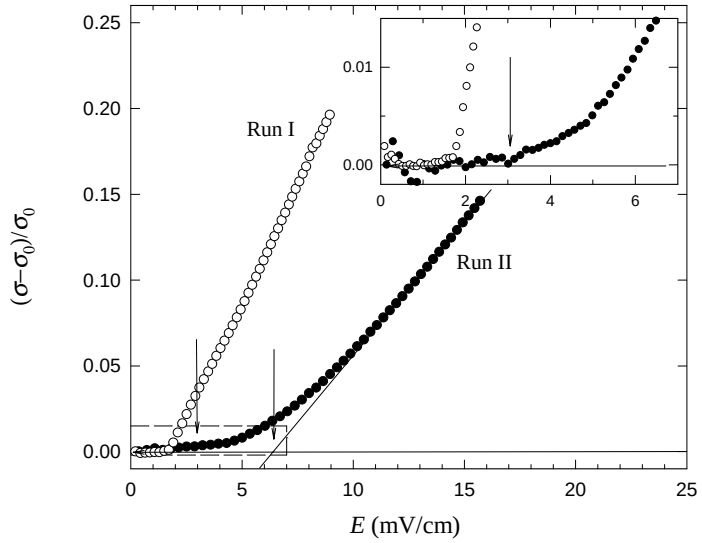

Fig. 1. The SDW excess conductivity $(\sigma - \sigma_0)/\sigma_0$ vs. electric field E. Inset: the enlarged low-field window. The arrows mark the threshold region for run II (see text).

The Fourier spectra recorded between the inner contacts in run I are shown in Figs. 2 and 3, for DC currents between 50 μA and 1000 μA. As the current is increased from zero to a value above the threshold I_T ($I_T \approx 80$ μA, which corresponds to $E_T = 2.6$ mV/cm in the two-probe I–V experiment), a well-defined frequency and two higher harmonics appear. At higher current values, the position of the frequency increases. Note that at the same time the voltage level is clearly enhanced in the low-frequency side of the spectra. The frequency amplitude increases until $I \approx 2I_T$ is reached, and then it starts to diminish and disappears at currents higher than 1000 μA (i.e., $I > 10I_T$). The fundamental frequency is broader than the instrumental resolution (1.25 kHz for the range 20 Hz – 500 kHz) and at $I \approx 2I_T$ a full width at half maximum equals 6.4 kHz at 140 kHz.

The Fourier spectra of the conduction noise was also measured after the thermal cycling loop (run II) between the inner (frequencies denoted as IIi) and the outer (frequencies denoted as IIo) contacts. In Fig. 4 we show the noise spectra recorded at the outer terminals (i.e., between the ends of the sample). These data indicate the appearance of the two distinct frequencies (labeled as IIoa and b) at the critical current ($I_T = 130$ μA), but also that (for higher current values) three additional

frequencies (II oc, d and e) emerge from the enhanced voltage level at the low-frequency side. The broadening of the frequency II oa occurs at $I = 250$ μA, indicating the emergence of two independent oscillations very close in frequency. The noise spectrum disappeared for $I > 500$ μA.

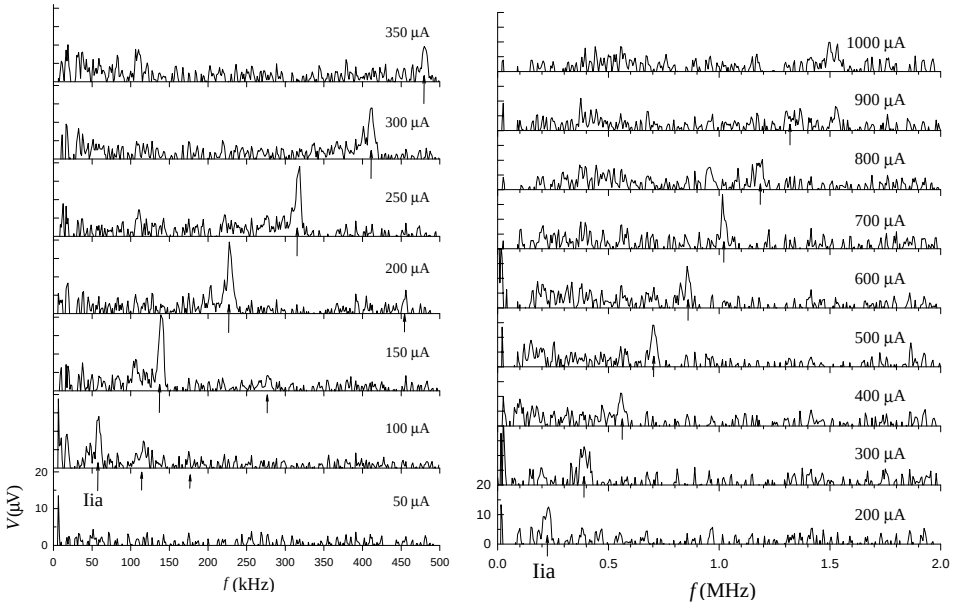

Fig. 2. The frequency spectra detected in run I between the inner contacts for selected values of the current. The frequency range: 0 – 500 kHz*. The arrows indicate the fundamental (I ia) and higher harmonics.*

Fig. 3 (right). The frequency spectra detected in run I between the inner contacts for selected values of current. The frequency range: 0 – 2 MHz*. The arrows indicate the fundamental (I ia) and higher harmonics.*

In the standard approach, the dynamics of DW is reduced to the variations of its phase (ϕ), while the amplitude fluctuations are frozen out. Its velocity is then given by [4]

$$v_{\mathrm{DW}} = \frac{\mathrm{d}\phi}{\mathrm{d}t}\lambda_{\mathrm{DW}} = f\lambda_{\mathrm{DW}}\,, \tag{1}$$

where λ_{DW} is the DW wavelength, and the phase rate $\mathrm{d}\phi/\mathrm{d}t$ is denoted as the frequency f. Taking into account that the coupling of the SDW to the impurity potential is controlled by $4k_{\mathrm{F}}$ periodicity, we can express the SDW collective current as

$$\frac{I_{\mathrm{SDW}}}{s_{\mathrm{eff}}} = (en\,\rho_{\mathrm{SDW}})f\frac{\lambda_{\mathrm{SDW}}}{2}\,, \tag{2}$$

where s_{eff} is the effective cross-section through which SDW current flows, en is the

total charge per unit cell and ρ_{SDW} is the fraction of electrons belonging to the SDW condensate. ρ_{SDW} varies between 1 and 0 (for $0 < T < T_c$), and its temperature variation is given by the temperature development of the order parameter Δ.

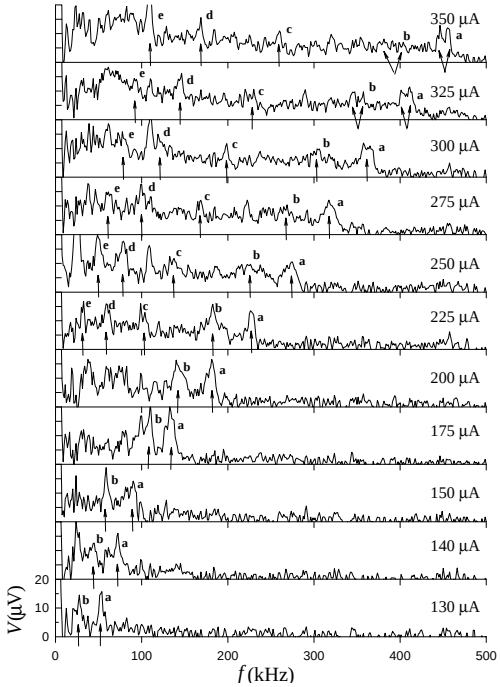

Fig. 4. The frequency spectra detected in run II between the outer contacts for selected values of current. The frequency range: 0 – 500 kHz. *The arrows indicate five different fundamentals (I ia-e).*

From the NMR and conductivity data [26,27] for $(\mathrm{TMTSF})_2\mathrm{PF}_6$, it is known that Δ rapidly increases below T_c and attains its zero temperature value at 4.2 K, and that the entire SDW condensate participates in the electric transport [18,19]. Therefore, we will take $\rho_{\mathrm{SDW}} = 1$ in further analysis, and Eq. (2) can be written ($C = s_{\mathrm{eff}}\, en\, \lambda_{\mathrm{SDW}}/2$) as

$$I_{\mathrm{SDW}} = Cf\,. \tag{3}$$

On the other hand, the phase slip theory predicts essentially the same expression for the collective current as a function of frequency at $T = 0$ K, but with a different prefactor [28]

$$I_{\mathrm{SDW}} = \eta C_1 f\,, \tag{4}$$

where $C_1 = 2C$. This is interesting to note, because in these theories the condition $d\phi/dt = 0$ (at the conversion point) imposes the importance of simultaneous

variations of the DW amplitude. The prefactor η is due to the diffusive process responsible for the generation of the phase slip. The constant C_1 is two times larger than in the impurity model, since each phase slip changes the phase by $2k_{\mathrm{F}}$. We proceed with the analysis of our data using Eq. (3), but bearing in the mind that it is valid in both theoretical models up to the prefactor 2η.

The analysis of our experimental data leads directly to the most important result we have obtained: the observed frequency dependence of I_{SDW} is not linear and its slope is, even at the highest fields used, much smaller than the theoretically predicted one. Figures 5 and 6 show the SDW current as a function of frequency

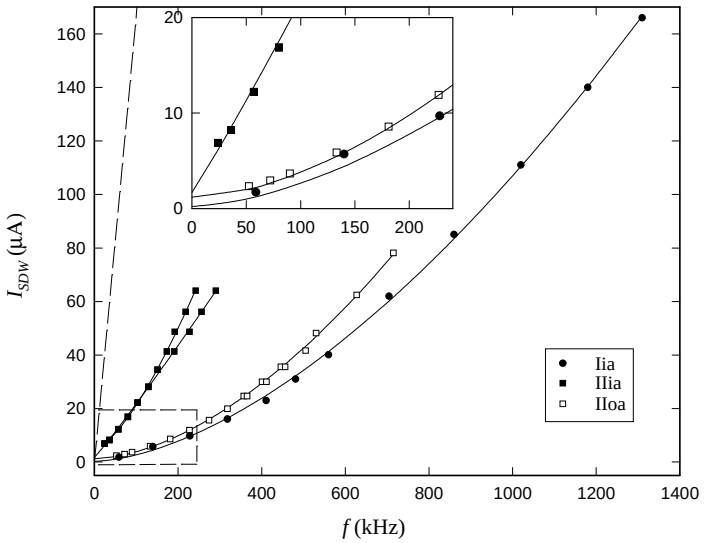

Fig. 5. Excess current I_{SDW} versus frequency f for the fundamentals Iia, IIia and IIoa, detected in runs I and II. Inset: the enlarged low- field window. Solid lines: fits by Eq. (6); dashed line: theoretical prediction (see text).

(observed in the Fourier spectra). The dashed line is the behaviour expected from Eq. (3), and its slope ($1.66 \cdot 10^{-9}$ C) was calculated by taking $s_{\mathrm{eff}} = s = 10^{-4}$ cm^2 (i.e., the whole sample cross-section), $n = 1.44 \cdot 10^{21}$ cm^{-3}, $e = 1.6 \cdot 10^{-19}$ C and $(1/2)\lambda_{\mathrm{SDW}} = (1/2)4a = 0.72$ nm. The solid lines drawn through our data are the fitting curves using a power law

$$I_{\mathrm{SDW}} = a + bf^n \,. \tag{5}$$

The values of the exponent n and the values of I_{SDW}/f ratio (obtained from the linear extrapolation of several points at the highest fields for which the Fourier peaks can still be detected) are given in Table 1.

The observed non-linear behaviour of I_{SDW} contrasts the predictions of both theoretical models. It indicates that the effective cross-section increases with an applied electric field, i.e., $s_{\mathrm{eff}} = s_{\mathrm{eff}}(E)$, which is, even at the highest fields applied,

much smaller than the sample cross-section. The exponent n might be interpreted as a measure of the effective cross-section change with the applied field (where larger n means faster increase of $s_{\rm eff}$, and $n = 1$ corresponds to the case when $s_{\rm eff}$ is field independent). On the other hand, the values of $I_{\rm SDW}/f$ ratio reveal the

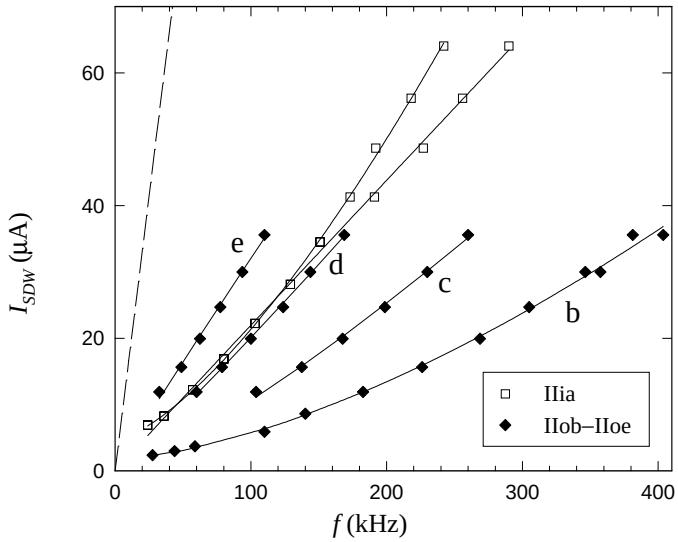

Fig. 6. Excess current $I_{\rm SDW}$ versus frequency f for the fundamentals $II ob$, $II oc$, $II od$ and $II oe$, detected in run II. Solid lines: fits by Eq. (6); dashed line: theoretical prediction (see text).

TABLE 1. The exponent n derived from $I_{\rm SDW} = a + bf^n$ and the final slope $\mathrm{d}I_{\rm SDW}/\mathrm{d}f$ estimated at $I_{\rm max}/I_T$ for different fundamentals observed in runs I and II. l and h denote the low and high frequency branch after splitting.

		n	$I_{\rm max}/I_T$	$\mathrm{d}I_{\rm SDW}/\mathrm{d}f(10^{-10}\mathrm{C})$
I run	I ia	1.64	10	2.0
II run	II ia l	1.20	2.7	3.2
	II ia h	1.00	2.7	2.3
	II oa	1.67	4	1.8
	II ob	1.42	2.7	1.2
	II oc	1.25	2.7	1.9
	II od	1.08	2.7	2.2
	II oe	0.97	2.7	3.4

magnitude of the effective cross-section at the highest fields applied. Our data show that the largest transverse effective volume amounts to about 10^{-5} cm^2 at different

values of applied fields (i.e., $E_{\max}/E_c$) in different samples. This result indicates that the upper limit of the transverse coherence of the SDW sliding conduction in the real samples is of the order of a few hundred micrometers. It should be noted that this result describes the dynamical coherence length as it was first introduced by Fisher [22]. Later, it was suggested by Ong et al. [23] that the dynamical coherence length is limited by phase slip centres, but still expected to be much larger than the static coherence length controlled by the density of pinning centres [24]. Indeed, our result demonstrates that the former is at least hundred times larger than the latter, which is estimated to be a few micrometers [24]. Moreover, our finding then suggests that the periodicity of the voltage oscillations should be $2k_{\mathrm{F}}$, as predicted by the phase-slip model. We point out that a qualitatively similar (non-linear) behaviour is observed in the CDW conduction as well, but this has only recently been recognized to be an intrinsic behaviour [29]. These authors have shown that even for very clean samples the slope $\mathrm{d}I_{\mathrm{SDW}}/\mathrm{d}f$ becomes saturated only at high frequencies (high fields), when s_{eff} becomes equal to the whole sample cross-section. Bearing in mind, however, that the typical cross-sections of $NbSe_3$ crystals ($10^{-8} - 10^{-7}$ cm^2) are much smaller than those of $(TMTSF)_2PF_6$ crystals ($4.5 \cdot 10^{-5} - 1.5 \cdot 10^{-4}$ cm^2), it follows that the SDW coherent conduction channels are even larger than the CDW ones. This finding indicates that a spatially restricted coherent conduction might be an intrinsic property of the sliding density waves in general.

The described experimental features show that the theoretically predicted behaviour (Eqs. (3) and (4)) account only for the high-field limit of the SDW coherent conduction. The fact that the largest possible SDW conduction channels are smaller than the cross-sectional area of the samples appears as a decisive shortcoming, which does not allow to measure the pertinent SDW periodicity by the joint conduction noise and DC electric transport method. In the discussion which follows we shall compare the other experimental features with the theoretical predictions, in order to try to distinguish which mechanism (phase slippage or interaction with random impurities) might be more relevant for the SDW dynamics.

First, we address the question of the field-dependence of the voltage oscillations. The periodicity of three fundamentals I ia, I I ia and I I oa as a function of field is shown in Fig. 7. The data have been fitted by a power-law behaviour

$$\frac{1}{f} \propto (E - E_c)^{-\beta} . \tag{6}$$

The best fits, together with the values of free parameters are shown as full lines in Fig. 7. The obtained values for E_c correspond well to those found in the noise measurements. The exponent $\beta \approx 1$ agrees well with the predictions of the impurity model. On the other hand, we could not test the validity of the phase slip model prediction, because it is obtained only in the limit when the size effects are important, i.e., when the threshold defined by boundary conditions is larger than the bulk threshold [7]. The samples used in our study were rather long and we did not observe the difference in the threshold field for non-linearity as a function of the length.

Second, thermal recycling of the sample leads to smaller magnitudes of the single fundamental frequencies IIia and Iioa, and they may be tracked in a smaller current window than the Iia frequency. Moreover, IIia and IIoa peaks split as the current increases above 300 μA. These features can be well understood in the framework of the phase slip theory as a consequence of the local field variations in the sample [30]. The field variations might be induced by the thermal gradient (well-known experiments in CDW) or by the sample inhomogeneities caused by the thermal cycling (like in our case). The first manifestation is the rounding off of $I-V$ characteristics, thus reflecting a gradual depinning. The other manifestations of the weak local field variations are visible in the noise spectra. For a large enough field variation, the frequencies of phase slips at the end contacts, i.e., fixed boundaries, start to differ, and this is observed as a splitting of the fundamental frequency. In order to accommodate this difference in the phase accumulation at the end contacts, a system generates so-called bulk phase slips at the free boundaries situated in the interior of the sample bulk. Theoretically, the new frequency is given by the difference of two split peaks and should be, therefore, visible at low frequencies.

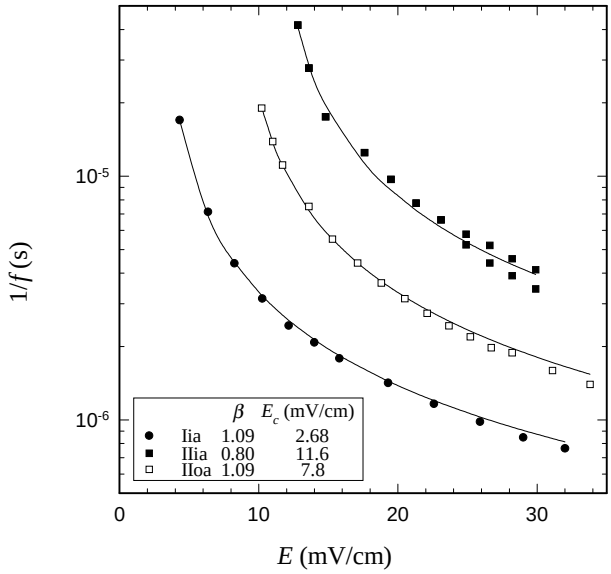

Fig. 7. The phase slippage period $1/f$ vs. electric field E for the highest fundamentals (Iia, IIia and IIoa). Full lines: fits by Eq. (6) (see text).

Further, as the DC current increases, new fundamentals emerge between outer terminals from the strongly enhanced voltage level in the low-frequency side. These frequencies might be associated with the opening of the new SDW conduction channels characterized by smaller velocities, but larger effective cross-sections. The existence of five independent fundamentals (cf. Fig. 4) indicates the presence of the phase-slip centres (inside the bulk of the sample) which act as fixed boundaries. Note also that the IIod fundamental might be identified with the higher branch of the IIia one, indicating the opening of the same conduction channel (Fig. 6).

Therefore, the phase-slip centres, at which all other frequencies (II oa, b, c, e) are generated, are located at the outer and inner terminals, and in the sample volume in between. The strongly enhanced voltage level of the low-frequency side (higher than the one observed between the inner terminals) might be also associated with these sample inhomogeneities, and interpreted as the growth of low velocity contributions when the electric field is increased. In addition to the new fixed boundaries that become active, the process of multiple splitting (due to the growing difference in the phase slip periodicities at different centres) creates new free boundaries. Note that this low-frequency noise does not obey the $1/f$ dependence, a common feature of the broad-band noise in CDW systems.

Finally, we present data which indicate that the phase slip process might indeed be the origin of the SDW conduction noise. Figure 8 shows I_{SDW} versus applied DC current for two different samples (A and B) and in two configurations. In the standard four-probe N configuration, the current flows between the outer, and the

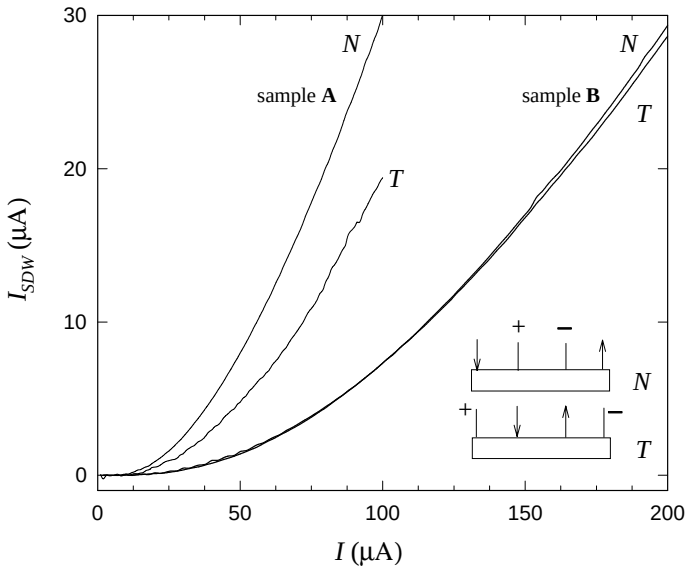

Fig. 8. The SDW current I_{SDW} vs. applied current I, for samples A (coherent noise observed) and B (no coherent noise observed). Measurements were done in two different four-probe configurations N and T (current: arrows, voltage probes: + and -).

voltage is measured between the inner terminals, whereas in the T configuration the current flows between the inner and the voltage is measured between the outer terminals. For the CDW systems Gill [31] has recently argued that the difference $I_{\mathrm{SDW}}(N) - I_{\mathrm{SDW}}(T)$, for a given I, gives the excess voltage V_{exc} which might be correlated to the phase slip process. Following the same arguments, we emphasize that V_{exc} has a finite positive value in the sample A (where a coherent noise was observed), whereas in the sample B, V_{exc} is close to zero (and no coherent Fourier peaks were found).

3.2. The magnetic field dependence of the threshold field

We have already mentioned that the transverse magnetic field influences the threshold field and that these results can be the measure of the deviation from the perfect nesting of the SDW state. In extension of the previous investigations [21,25], we have studied the magnetic field dependence of the threshold field E_T for $(TMTSF)_2PF_6$ at 4.2 K, at ambient pressure and in magnetic fields up to 6 T.

Figure 9 presents the dependence of the threshold field E_T (normalized to its $B = 0$ value) as a function of the transverse magnetic field (which was parallel to the least-conductivity direction **c***). Also shown are the previously obtained results [21] for $(TMTSF)_2NO_3$, which were interpreted in terms of the Bjeliš-Maki model with the imperfect nesting within the mean field theory [24]. Bjeliš and Maki have shown that a magnetic field perpendicular to the conducting plane strongly reduces the

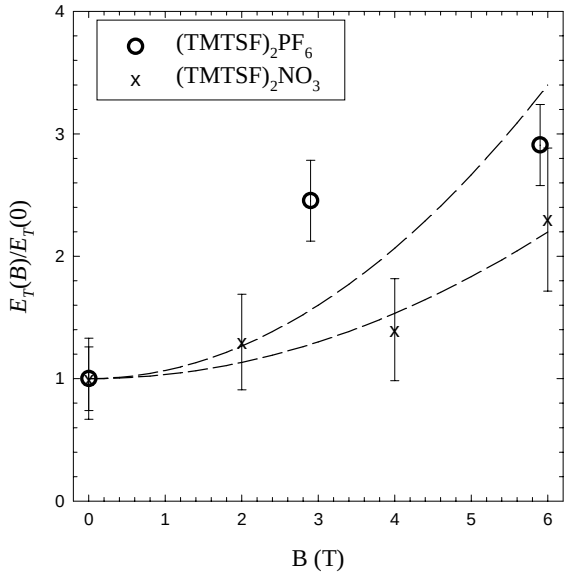

Fig. 9. The magnetic field dependence of the threshold electric field E_T normalized to $B = 0$ value at 4.2 K *for* $(TMTSF)_2PF_6$. *The crosses are data for* $(TMTSF)_2NO_3$ *[21].*

elastic constant, i.e., the energy associated with a spatial distortion of the phase is reduced. This results in an increase of the fluctuation contribution to the transport properties in a magnetic field. In the SDW with imperfect nesting, the decrease of the elastic constant increases the threshold electric field. Consequently, both the longitudinal and transverse coherence lengths are reduced in an applied magnetic field. Our results (cf. Fig. 9) show that the threshold field E_T of $(TMTSF)_2PF_6$ increases in the applied magnetic field, which indicates the existence of some degree of imperfect nesting in this system as well. The parameter ϵ_0 that characterizes the imperfect nesting effect is associated with the quasi-one dimensionality of the system. It is defined as $\epsilon_0 = t_b^2/2t_a$, where t_a and t_b are the tight binding transfer

integrals for the **a** and **b** axis. The deviation from the perfect nesting is described by ϵ_0/Δ_0, where Δ_0 is the order parameter of the hypotetical SDW with perfect nesting ($\epsilon_0 = 0$) at $T = 0$ K.

The magnitude of the threshold field is given by the energy for which the static electric field overcomes the pinning energy and thus dislodges the SDW from the background lattice. The change of the threshold field in an applied magnetic field (in the strong pinning limit) is given by [32]:

$$\frac{E_T(B)}{E_T(0)} \approx 1 + \frac{4}{3}x^2y^2(3 - 5y^2)\,, \tag{7}$$

where $x = \omega_C/\Delta_0$ ($\omega_C = vbeB$ is the cyclotron frequency, v is the Fermi velocity, b is the lattice parameter in the **b** direction, B is the magnetic field in the **c** direction) and $y = \epsilon_0/\Delta_0$ is the deviation from the perfect nesting.

Using the same parameters as for $(TMTSF)_2NO_3$ (i.e., $v \simeq 3{\cdot}10^7$ cm/s, $\Delta_0 \simeq 20$ K), we have fitted our data by Eq. (7) (shown as a dashed line in Fig. 9). The final result for $(TMTSF)_2PF_6$ obtained in this way is $\epsilon_0/\Delta_0 \approx 0.94$. Bearing in mind our previous result for $(TMTSF)_2NO_3$ ($\epsilon_0/\Delta_0 \approx 0.97$) [21], as well as the results for the pressure and magnetic dependence of the order parameter and SDW transition temperature [25], we can conclude that $(TMTSF)_2PF_6$ is imperfectly nested at ambient pressure. The deviation from the perfect nesting is, as expected, less pronounced than in $(TMTSF)_2NO_3$.

3.3. The nonlinear Hall effect

It was often assumed that the transport coefficients of the thermally excited normal electrons should be the same in the pinned and depinned SDW state. From this point of view, no SDW contribution is expected to the Hall effect, because of the strictly 1D nature of the density wave transport. On the other hand, the experimental results clearly show that the Hall resistivity becomes non-linear when the SDW is depinned [33,34]. Our results for $(TMTSF)_2PF_6$ demonstrate also a similar behaviour. In Fig. 10, the longitudinal resistance R_L and the Hall resistance R_{xy} are shown as a function of the total current I at 4.2 K for several magnetic field values. It can be seen that above critical current the resistance R_L decreases, thus defining the threshold field. In addition, as soon as R_L decreases, the Hall resistance R_{xy} decreases as well and shows a slightly steeper nonlinearity. It is apparent that V_H/I falls faster than V_L/I above the threshold, i.e., V_H/V_L is reduced. Such an effect was considered as an indication that the SDW does give a contribution to the Hall effect [35].

When the applied electric fields are below the threshold value, the Hall resistivity is linear with the magnetic field. The negative sign of the Hall coefficient indicates that the charge carriers are electrons. Using the simple relation for the Hall coefficient $R_H = \rho_{xy}/B = 1/nec$, we get $R_H = -25$ cm^3/C and the corresponding carrier concentration $n \approx 10^{17}$ cm^{-3}, which is in a good agreement with the data for some other Bechgaard salts [36].

The existence of a well-defined threshold field (for higher electric fields applied) indicates that the sliding SDW contributes to the Hall effect. In their theoretical model [35], Artemenko and Kruglov propose that this contribution is indirect, because the motion of the SDW alters the current carried by the normal electrons. Namely, the defect scattering modifies the quasiparticle distribution and leads to a change in the transport coefficients. In the simplest terms of this theory, this means that there is a decrease of the normal (quasiparticle) current I_N which is proportional to the sliding velocity of the SDW, i.e., the motion of the SDW induces an additional and reversed normal current. The total current I_T can then be written as

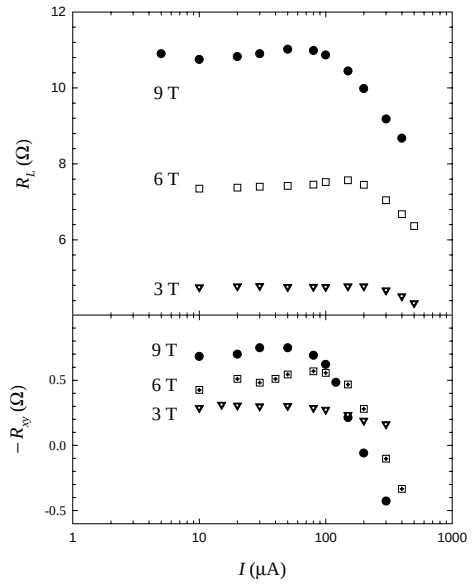

Fig. 10. The current dependence of the resistance R_L and the Hall resistance R_{xy} for different values of the magnetic field.

$$I_T = I_N - \alpha I_{\mathrm{SDW}} + I_{\mathrm{SDW}} \,, \tag{8}$$

where I_{SDW} is the current carried by the SDW and $\alpha I_{\mathrm{SDW}} = I_b$ is the backward normal current flow with an adjustable parameter α called the 'backflow' coefficient. Figure 11 presents the total current and the normal current as a function of the longitudinal voltage V_L of the sample in a magnetic field of 9 T, and we shall use these data to calculate the backflow coefficient α. The threshold field $E_T \approx 15$ mV/cm corresponds to $V_L \approx 0.6$ mV. The total current I_T is measured directly on the longitudinal voltage contacts. Taking the linear extrapolation of the low-field current as I_{LIN}, and deducing the normal current I_N from the measured Hall voltage V_H ($I_N = V_H/R_{xy}$) as $I_N = I_{\mathrm{LIN}} - I_b$, enables one to determine the backflow current I_b and the value for the backflow coefficient α. We have found $\alpha = 0.92 \pm 0.05$, which is a very high value (several orders of magnitude higher than in the theoretical

model), but only two times higher than in the case of $(TMTSF)_2AsF_6$ [33]. The theoretical model [35] does not take into account the Coulomb interaction between the SDW and the normal electrons, and it was proposed [33] that the Coulomb effects might enhance the backflow coefficient. Since the high values of α were also found in some CDW systems [34], we suggest that the large backflow of normal carriers is an intrinsic property of quasi-1D systems, and a consequence of the interaction between the normal carriers and the moving SDW. On the other hand, the widely studied theory of the nonlinear Hall effect in the field induced SDW by Yakovenko et al. [37] is restricted to the extreme quantum limit and not applicable to our ambient pressure data.

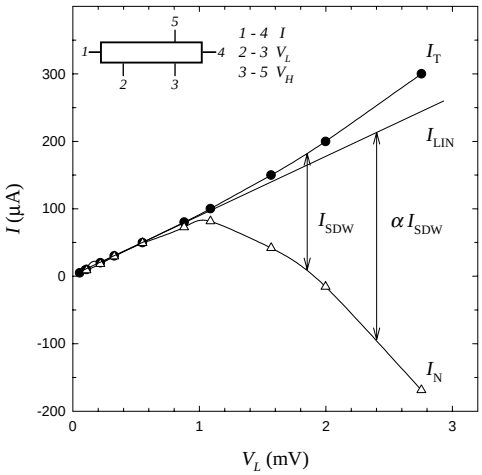

Fig. 11. The total current density I_T, normal current density I_N and SDW current density I_{SDW} as a function of longitudinal voltage V_L at 4.2 K *and in the magnetic field of 9* T*. Also shown is a sketch of the sample geometry (the distance between the voltage contacts was 0.04* cm*).*

4. Summary

We have presented a detailed experimental study of the oscillation phenomena and the influence of the magnetic field in spin-density wave transport. For the first time we have clearly shown that the Fourier spectra consist of sharp discrete frequencies and an enhanced voltage level at the low-frequency side. In very pure samples with a sharp threshold field, the SDW motion is characterized by nearly perfect spatial coherence of velocity. The space in which the SDW slides increases gradually in size until the maximum possible channel's cross-section of about 10^{-5} cm^2 is achieved. The latter indicates that the transverse dynamical coherence length is about 100 times larger than the static one. Concomitantly, for fields above twice the threshold, the spatial coherence starts to diminish. Such a process indicates the crucial role of inhomogeneities in the real samples. In the presence of an increased defect content, novel channels open, which are characterized by smaller velocities and larger cross-sections. The observed decrease of the Fourier peak amplitude with

the associated broadening and multiple splitting support the phase slip model developed for CDW. This phenomenon might also be responsible for the simultaneous development of the low-frequency noise.

As for the effect of the magnetic field, we have interpreted the increase of the threshold field in the transverse magnetic field as a confirmation that the Fermi surface is imperfectly nested. The Hall-effect measurements at low electric field yield the electrons as the charge carriers, and their concentration at 4.2 K is $\approx 10^{17}$ cm^{-3}. For higher electric fields, the SDW is depinned, and the Hall resistivity becomes nonlinear. The calculated high value of the backflow coefficient α might be ascribed to the Coulomb interactions.

Acknowledgements

The samples used in this work were provided by K. Bechgaard. We have benefited from discussions with J. Richard in the early stage of the conduction noise study. We acknowledge the participation of N. Francetić in the Hall-effect studies and the useful discussions with A. Bjeliš, D. Jelčić, K. Maki and M. Prester.

References

1) *Low-Dimensional Conductors and Superconductors*, ed. D. Jérome and L. G. Caron, NATO Adv. Study Inst., Series B, Vol. 155, Plenum, New York (1987); G. Grüner, Rev. Mod. Phys. **60** (1988) 1129;

[2] S. Tomić, J. R. Cooper, D. Jérome and K. Bechgaard, Phys. Rev. Lett. **62** (1989) 462; G. Grüner, Rev. Mod. Phys. **66** (1994) 1;

[3] H. Fukuyama and P. A. Lee, Phys. Rev. B **17** (1978) 535; P. A. Lee and T. M. Rice, Phys. Rev. B **19** (1979) 3970;

[4] A. Bjeliš, in *Low-Dimensional Conductors and Superconductors*, ed. D. Jérome and L. G. Caron, NATO Adv. Study Inst., Series B, Vol. 155, Plenum, New York (1987) p. 409;

[5] H. Matsukawa and H. Takayama, Jpn. J. Appl. Phys. **26**, Suppl. 26-3 (1987) 601;

[6] L. P. Gorkov, JETP Lett. **38** (1983) 87; JETP **59** (1985) 1957;

[7] I. Batistić, A. Bjeliš and L. P. Gorkov, J. Physique **45** (1984) 1049;

[8] N. P. Ong, G. Verma and K. Maki, Phys. Rev. Lett. **52** (1984) 663;

[9] S. N. Artemenko, A. F. Volkov and A. N. Kruglov, Sov. Phys. JETP **64** (1987) 906;

[10] D. Feinberg and J. Friedel, J. Physique **49** (1988) 485;

[11] D. Jelčić and A. Bjeliš, Fizika A **1** (1992) 93;

[12] I. Bloom, A. C. Marley and M. B. Weissman, Phys. Rev. Lett. **71** (1993) 4385;

[13] A. C. Marley, I. Bloom and M. B. Weissman, Phys. Rev. B **49** (1994) 16156;

[14] I. Bloom, A. C. Marley and M. B. Weissman, Phys. Rev. B **50** (1994) 5081;

[15] K. Nomura, T. Shimizu, K. Ichimura, T. Sambongi, M. Tokumoto, H. Anzai and N. Kinoshita, Solid State Commun. **72** (1989) 1123;

[16] N. Hino, T. Sambongi, K. Nomura, M. Nagasawa, M. Tokumoto, H. Anzai, N. Kinoshita and G. Saito, Synth. Met. **40** (1991) 275;

[17] G. Kriza, G. Quirion, O. Traetteberg, W. Kang and D. Jérome, Phys. Rev. Lett. **66** (1991) 1922;

[18] E. Barthel, G. Kriza, G. Quiron, P. Wzietek, D. Jérome, J. B. Christensen, M. Jørgensen and K. Bechgaard, Phys. Rev. Lett. **71** (1993) 2825;

[19] W. G. Clark, M. E. Hanson, W. H. Wong and B. Alavi, Phys. Rev. B **49** (1994) 11985;

[20] For a review see: T. Ishiguro, K. Yamaji, *Organic Superconductors*, Springer-Verlag, Berlin (1990);

[21] N. Biškup, M. Basletić, S. Tomić, B. Korin-Hamzić, K. Maki, K. Bechgaard and J. M. Fabre, Phys. Rev. B **47** (1993) 8289;

[22] D. S. Fisher, Phys. Rev. Lett. **50** (1983) 1486;

[23] N. P. Ong and K. Maki, Phys. Rev. B **32** (1985) 6582;

[24] A. Bjeliš and K. Maki, Phys. Rev. B **44** (1991) 6799;

[25] N. Biškup, S. Tomić and D. Jérome, Phys. Rev. B **51** (1995) 17972;

[26] S. Tomić, J. R. Cooper, W. Kang, D. Jérome and K. Maki, J. Phys. I (France) **1** (1991) 1603;

[27] T. Takahashi, Y. Maniwa, H. Kawamura and G. Saito, J. Phys. Soc. Jpn. **55** (1986) 1364;

[28] A. Bjeliš, in *Applications of Statistical and Field Theory Methods to Condensed Matter*, ed. D. Baeriswyl, A. R. Bishop and J. Carmelo, NATO Advanced Study Institute, Series B, Vol. 218, Plenum, New York (1990) p. 325;

[29] J. Richard, J. Chen and S. N. Artemenko, J. Physique IV C2 **3** (1993) 33;

[30] D. Jelčić and A. Bjeliš, Phys. Rev. B **43** (1991) 1735;

[31] J. C. Gill, Phys. Rev. Lett. **70** (1993) 331;

[32] K. Maki, Phys. Rev. B **47** (1993) 11506;

[33] O. Traetteberg, L. Balicas and G. Kriza, J. Phys. IV (France) **3** (1993) C2-61;

[34] L. Forro, J. R. Cooper, A. Janossy and M. Maki, Solid State Comm. **62** (1987) 715;

[35] S. N. Artemenko and A. N. Kruglov, Fiz. Tver. Tela **26** (1984) 2391p;

[36] M. Basletić, B. Korin-Hamzić, A. Hamzić, S. Tomić and J. M. Fabre, Solid State Comm. **97** (1996) 333;

[37] N. Dupuis and V. M. Yakovenko, Europhys. Lett. **45** (1999) 361.

KLIZNI VALOVI SPINSKE GUSTOĆE: PROUČAVANJE STRUJNOG ŠUMA, OVISNOSTI O MAGNETSKOM POLJU I HALLOVOG OTPORA

Proučavali smo karakteristike napon – struja materijala $(TMTSF)_2PF_6$ u stanju valova spinske gustoće (SDW). Za oscilatorni dio nelinearnog naponskog odziva na istosmjerno električno polje, osnovna frekventna raspodjela (kao funkcija tog polja) i nelinearan odnos frekvencije i SDW struje pokazuju rast usporednih kanala vođenja označenih manjim brzinama i većim udarnim presjecima. Broj osnovnih frekvencija, njihove amplitude i razina niskofrekventnog šuma, kao i otkočno ponašanje sustavno pokazuju na nehomogenosti uzorka i pridružene varijacije lokalnog polja, i mogu se shvatiti u okviru modela klizne faze. Rast praga električnog polja s magnetskim poljem može se protumačiti Bjeliš-Makijevom teorijom, ako se uzme u obzir ugniježdenje. Konačno, nalazimo da je ovisnost Hallovog otpora o električnom polju u skladu s kliznim mehanizmom SDW vođenja struje.